POWDER-BASED FUNCTIONAL MATERIALS FOR EXTREME ENVIRONMENTS: PROCESSING AND CHARACTERIZATION

Thermal Conductivity and Microstructure of Cu-Coated Graphite Flake/Ti Alloy Composites Fabricated by Spark Plasma Sintering

ZUNYUE YU,[1] JINKUN QI,[2] WENRU ZHAO,[1] XUEPENG REN,[1] YANG ZHAO,[1] SHUBIN REN,[1,3] and XUANHUI QU[1]

1.—Beijing Advanced Innovation Center for Materials Genome Engineering, Institute for Advanced Materials and Technology, University of Science and Technology Beijing, Beijing 100083, China. 2.—Hebei Wuwei Aero&Power Technology Co., Ltd, Zhangjiakou 075600, China. 3.—e-mail: sbren@ustb.edu.cn

Graphite flake (GF)-reinforced Ti6Al4V (TC4) matrix composites were fabricated by spark plasma sintering, and electroless copper (Cu) plating on the surface of the GFs was introduced to slow the interface reaction between the GFs and the TC4 and to improve the interface bonding. The effects of sintering temperature and coating thicknesses on the microstructure and thermal conductivity (TC) of the composites were investigated. The results showed that the introduction of the Cu coating can significantly reduce the thickness of the titanium carbide (TiC) layer generated by the interface reaction between the GFs and the TC4, increase the density of TiC layer, and thus increase the TC of the composite. When the sintering temperature was below 1150°C, the TC gradually increased from 185.03 W m^{-1} K^{-1} before Cu plating to 232.4 W m^{-1} K^{-1} with the increase of the Cu coating thickness and sintering temperature. When the temperature was further increased to 1200°C, the TC deteriorated due to the increase in the thickness of the TiC layer. The high TC makes the GF/TC4 composites suitable candidates for heat transfer materials used in offshore engineering.

INTRODUCTION

A plate heat exchanger (PHE) has the characteristics of high heat exchange efficiency, small heat loss, compact and lightweight structure, small floor area, long service life, etc. It has become an essential heat exchange equipment for marine engines.[1–5] PHE is composed of a group of rectangular heat transfer plates made of thin metal, and the performance of the plates has an important impact on the heat transfer efficiency, service life, and applicable working conditions of the PHE.[3,6] Under most working conditions, metal plates are usually made of aluminum (Al) or copper (Cu) because they have high thermal conductivity (TC). Considering the corrosivity of the marine environment, due to the poor corrosion resistance of Al or Cu, the PHEs used in marine ships are mainly made of pure titanium (Ti) or Ti alloys with excellent corrosion resistance.[1,3,7–11] With the increasing power of marine turbines, it has become necessary to further improve the heat transfer efficiency without increasing the volume of the PHE. In particular, it is hoped that the plate has a high TC in the two-dimensional plane direction to enable the rapid exchange of heat between the sea water and the working medium in the plane, so as to improve the heat transfer efficiency.[2,3] The current TC of Ti and Ti alloy plates is too low to meet the comprehensive performance requirements of high-power marine turbines for PHEs.[12–14] How to improve the TC of Ti in a two-dimensional plane is a key problem that must be solved when it is used in high-power marine engines and other heat exchange equipment under similar working conditions.

Thermal Conductivity and Microstructure of Cu-Coated Graphite Flake/Ti Alloy Composites Fabricated by Spark Plasma Sintering

1263

In recent years, there has been much research on high-TC materials, mainly focusing on the field of electronic packaging, to solve the heat dissipation problem of high-power microwave devices and LED chips.[15–17] The materials developed include Cu matrix composites, Al matrix composites, such as diamond/Cu, graphite flake/Cu (GF/Cu), and diamond/Al.[18–21] These materials have been developed by adding a second component with high TC, such as diamond and GFs, to Al or Cu to solve the problem of low TC and excessive thermal expansion coefficient of Cu or Al. Although these high-TC composites cannot be applied in the marine environment due to their poor chloride ion corrosion resistance,[22] the relevant improvement methods proposed for the lack of thermophysical properties of single materials such as Cu or Al, e.g., the method of adding a high-TC second phase to make up for the lack of thermophysical properties of single materials, have a important reference value for improving the TC of Ti alloys. In other words, for Ti materials, the TC can also be improved by adding high-TC components such as diamond and GFs. The second phases used to improve the TC of metals reported in the literature are mainly carbon-based materials with high TCs, including diamond,[23–25] graphene,[26,27] carbon nanotubes,[28–30] GFs,[16,17] etc. Among these materials, the high TC of GFs in the two-dimensional plane direction is up to $1000 \, \mathrm{W \, m^{-1} \, K^{-1}}$.[15,31,32] At the same time, they have good characteristics of a self-oriented parallel arrangement, good dispersion, and chloride ion corrosion resistance,[22,33,34] which makes an ideal second phase to improve the TC of Ti materials in the two-dimensional plane direction. This idea also coincides with the thinking of other scholars.[35]

In the early stage, we mixed 50 vol.% GFs with Ti6Al4V (TC4) powder and sintered them by spark plasma sintering (SPS) to obtain GF/TC4 composites. From the microstructure, it can be seen that GFs can be uniformly and parallel arranged in the TC4 matrix. The measured TC in the direction consistent with the arrangement of the GFs reached $185.03 \, \mathrm{W \, m^{-1} \, K^{-1}}$, which is more than 20 times that of the TC of the TC4 matrix itself. This means that it is feasible to increase the TC by adding GFs to the TC4 matrix. However, at the same time, we also found that there is an interface reaction at the interface between the GFs and the TC4, and a titanium carbide (TiC) layer with a certain thickness is formed. This layer has a large interface thermal resistance, which will lead to a low TC of the composite. A study has shown that heat transfer between the interfaces is important. Researchers have found that the interfaces are barriers to heat transfer and may be a limiting factor in the development of highly thermally conductive materials. Therefore, the interface between the metal and the reinforcing phase needs to be modified to increase the TC.[35] At present, the improvement of the interface between a high-TC reinforcement phase and the matrix is mainly focused on diamond-Cu,[21,36] GF-Cu,[20,32] and diamond-Al systems.[19,33] Different researchers have proposed different interface modification methods for these systems. However, there is no publicly reported method on how to improve the interface bonding between GFs and Ti alloys, reduce the thickness of the carbide layer, and even inhibit the interface reaction between them. On the basis of our previous results, we propose to coat Cu on the surface of the GFs and combine them with TC4 to fabricate GF/TC4 composites by SPS. It is expected that coating Cu on the GF surface can reduce the contact time between the GFs and the Ti matrix during sintering densification, so as to reduce the thickness of the carbide layer and improve the TC of the composite. This paper focuses on studying the influence of the thickness of the Cu plating and the SPS sintering temperature on the microstructure and TC of the prepared GF/TC4 composites by a variety of material analysis and testing methods.

EXPERIMENTAL

Raw Materials

GFs with a particle size of 500 μm, a thickness of 50 μm, and a density of 2.26 g cm^{-3}, purchased from Forsman Scientific, China, was used as raw material. Scanning electron microscopy (SEM) images of a GF are shown in Fig. 1a. A magnified image of the edge region of the GF is shown in Fig. 1b, which shows its laminar structure. The X-ray diffraction (XRD) pattern of the GF is shown in Fig. 1c. The two peaks at $2\theta = 26.4°$ and $54.5°$ correspond to the (002) and (004) crystal planes of the GF, respectively. Spherical TC4 powder was used as the matrix material (TC: $6.6 \, \mathrm{W \, m^{-1} \, K^{-1}}$).[12,14] The characteristics of the TC4 powder are listed in supplementary Table S-I (refer to online supplementary material). The morphology of the TC4 powder is shown in Fig. 1d.

Fabrication of Cu-Coated GF

Cu-coated GFs were fabricated by electroless Cu plating with steps of surface degreasing, chemical roughening, sensitization, activation, and chemical plating: (1) a GF was placed in an electric furnace at 400°C in air atmosphere for 30 min to remove surface organic matter and volatile impurities; (2) the GF was immersed in a hydrochloric acid solution to form a rough surface to increase the specific surface area, and then placed in an ultrasonic cleaner to be cleaned to neutral; (3) after roughening, the GF was sensitized in a hydrochloric acid solution of SnCl$_2$ (30 g L^{-1} for SnCl$_2$ solution and 60 mL L^{-1} for hydrochloric acid solution) and washed with deionized water to neutral; (4) the sensitized GF was activated in a 0.25-g L^{-1} PdCl$_2$ solution; (5) finally, the activated GF was used for electroless plating, and the composition of the plating solution is shown in supplementary Table S-II. In addition, NaOH solution was chosen
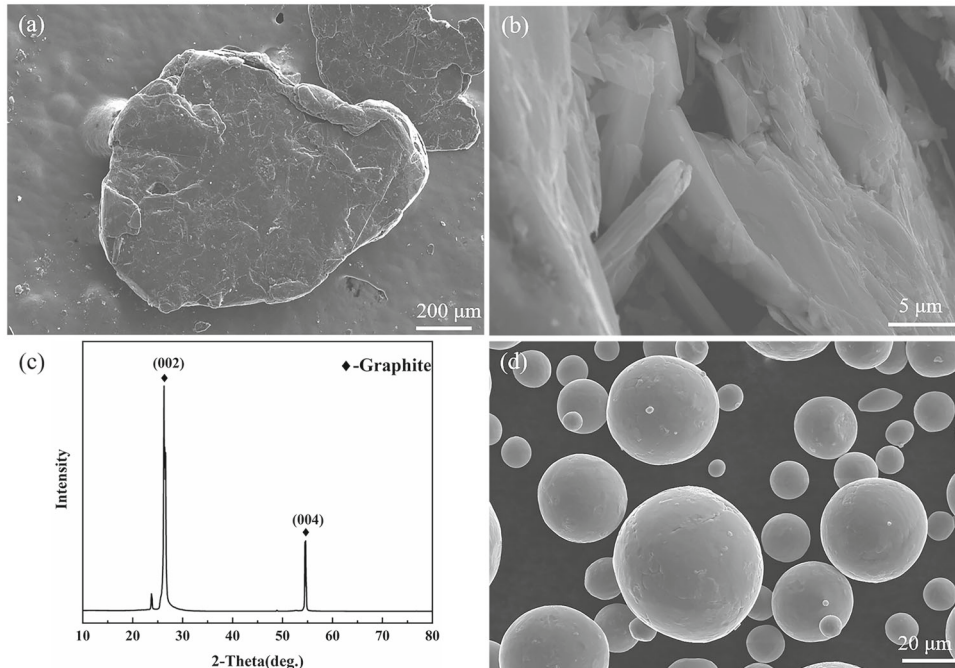
Fig. 1. SEM images and XRD pattern of raw materials: (a) overall view of a GF; (b) high magnification of the edge region of the GF; (c) XRD pattern of the GF; (d) SEM image of TC4 powder.

to adjust the pH of the solution to be stable at 12–13. The same quantity (6 g) of activated GF was added to different volumes (200, 400, and 800 mL) of Cu plating solution to obtain different layer thicknesses. The thickness of the coating increased with the increase of the plating volume. The coating thickness was determined by weighing the weight changes of the graphite flake before and after electroless copper plating. The formula for calculating the thickness of the Cu coating is:

$$\frac{\pi R^2 t}{\pi (R+d)^2 (t+2d) - \pi R^2 t} = \frac{V_{GF}}{V_{Cu}} \qquad (1)$$

$$V_{GF} + V_{Cu} = 1 \qquad (2)$$

where R is the radius of the graphite flake, t represents its thickness, V_{GF} refers to its volume fraction, V_{Cu} is the volume fraction of Cu, and d is the thickness of the coating. Through calculation, the thicknesses of the Cu coating on the surface of the GF corresponding to the three plating solution volumes was 550 nm, 1.3 μm, and 2.1 μm, respectively. The GF corresponding to different plating volumes were denoted as GCu200, GCu400, and GCu800, respectively.

After the coating was completed, we cleaned the GF with deionized water several times until the pH value of the cleaning solution was neutral. Then, the cleaned GF was dried in a vacuum drying oven for 1 h. Finally, the dried GF was kept at 250°C in hydrogen atmosphere for 2 h to reduce the effect of

hydrogen on the Cu coating. In the end, a GF coated with Cu (GCu) was obtained.

Fabrication of the Composites

First, the spherical TC4 powder was ball-milled into flakes. The flake matrix powder can make GFs with the same flake shape more parallel to each other in the matrix.[28,30,31] The morphology of the TC4 powder after ball milling is shown in supplementary Fig. S-1.

Then, 50 vol.% GF or GCu were dry-mixed with the flaked TC4 powder. After mixing, a certain amount of anhydrous ethanol (about 8% of the total volume of the powder) was added to make the TC4 powder adsorb on the surface of the GF. The two powders were then mechanically stirred to prevent uneven distribution of powders due to their large difference in density. Then, the mixed powder was filled into the mold several times. Each time, the powder needs to be pre-compacted under a certain pressure. After the powder-filling process was completed, we applied a pressure of 50 MPa to the filler and kept it for 2 min. During the pressure maintaining period, the GFs in the mixed powder can automatically arrange and tend to be parallel. At the same time, ethanol liquid was extruded from the mixture under pressure, and finally a cylindrical preform was obtained. The preform was then dried in a vacuum drying oven at 80°C for 12 h to obtain the final green body. In our previous exploration experiments, we found that the composites sintered at 1100–1200°C had a higher density. Therefore, the temperature of 1150°C was selected for the SPS

Thermal Conductivity and Microstructure of Cu-Coated Graphite Flake/Ti Alloy Composites
Fabricated by Spark Plasma Sintering

1265

sintering. GF/TC4, GCu200/TC4, GCu400/TC4, and GCu800/TC4 composites were prepared by using uncoated GFs and three kinds of GCus with different coating thicknesses (GCu200, GCu400, and GCu800) to investigate the effects of coating thickness on the orientation of the GFs (GCu), the TiC layer thickness, and the TC of the composites. The SPS sintering pressure was 30 MPa and the holding time was 5 min. In the sintering process, the GFs further tended to be arranged in parallel on the basis of the forming orientation of the preform under the effect of sintering pressure. As shown in the schematic in supplementary Fig. S-2, the arrangement direction is perpendicular to the pressure direction. The ideal arrangement is that the plane direction of all the GFs is parallel to the X–Y plane of the sample and perpendicular to the pressing direction.

GCu400/TC4 composites were selected to study the effects of sintering temperatures, 1050°C, 1100°C, 1150°C, and 1200°C, on the orientation of the GCu, the TiC layer thickness, and the TC of the composites.

Characterization of the Composites

Field-emission SEM (JSM-7001F; JEOL) was used to characterize the microstructure of the raw powder and the composites. The microstructure of the produced material was also quantitatively analyzed. The images used for the analysis were randomly selected from the surface of the samples and were used to calculate the continuity of the GFs. The continuity is the fraction of the total internal surface area shared by a certain phase with particles of the same phase.[37,38] The continuity can be expressed by:[37,38]

$$C_{\mathrm{M}} = \frac{2N_{\mathrm{MM}}}{2N_{\mathrm{MM}} + N_{\mathrm{MW}}} \quad (3)$$

where C_{M} is the continuity of the M phase, N_{MM} represents the numbers of M–M intercepts per unit length, and N_{MW} is the number of M–W intercepts per unit length.

The interface between the TC4 matrix and the GF(GCu) was further observed by field-emission transmission electron microscope (TEM; Tecnai G2 F20; FEI). The phase composition of the composite was determined by X-ray diffraction (XRD; D5000; Siemens). The element map distribution of the composites was characterized by energy dispersive X-ray spectroscopy (EDS). The TC values of the composites were calculated by $\lambda = \alpha \rho C_{\mathrm{P}}$, where λ was the TC of the composite, α was the thermal diffusivity, ρ was the density, and C_{P} was the specific heat. The thermal diffusivity and specific heat of the composites were measured by the laser flash method (LFA-467; Netzsch, Germany) with a sample size of 10 × 10 × 2 mm. The densities of the composites were measured by Archimedes' method. The TC of the composites prepared under different experimental conditions was tested with five specimens, and the average value was taken as the TC under the experimental conditions.

RESULTS AND DISCUSSION

Characterization of GCu

The macroscopic morphology of a GF before and after electroless plating is shown in Fig. 2a and b. Figure 2b shows the GF with a red Cu metallic luster. The microscopic morphologies of the GF after electroless Cu plating are shown in Fig. 2c–f. It can be seen from Fig. 2c that the surface of GF after Cu plating still presented a rough state, as shown in Fig. 1. From the EDS mapping of the GF surface shown in Fig. 2d, it can be seen that the Cu coating was evenly distributed on the surface of the GF without significant leakage. Further, it can be seen from the larger magnification images in Fig. 2e and f, that the Cu coating was composed of spherical particles.

Microstructure of Composites

Figure 3 shows the SEM images of the GF/TC4 and GCu/TC4 composites with different thicknesses of the Cu coating sintered at 1150°C. It can be clearly observed that the GF or GCu (black phase) can be uniformly dispersed in the TC4 matrix (dark gray phase) in the prepared composites. The plane directions of different GF particles were roughly parallel in the TC4 matrix, and their directions were basically parallel to the X–Y plane direction of the sample.

However, through careful comparison, it can be found that, in the GF/TC4 composites, shown in the red circle area in Fig. 3a, the angle between the orientation of some of the GFs and the X–Y direction was large, and that some GFs were even perpendicular to the X–Y plane direction. With the gradual increase of the Cu coating thickness, as shown in Fig. 3b and c, the angle became smaller. When the coating thickness exceeded 2 μm, as shown in Fig. 3c, the angle no longer changed significantly. This change in the angle between the orientation direction of some GFs and the direction of the sample plane (X–Y direction) may be related to the Cu plating on the surface of the GFs. First, the Cu plating on the GF surface was helpful in improving the strength of the GF and reducing its bending or fracture in the preforming or sintering process. From Fig. 3b–d, it can be seen that the GF kept its original disc shape, and almost no bending of the GF can be seen, as shown in Fig. 3a. Also, the Cu in the Cu plating layer became liquid phase at the sintering temperature, and so can play the role of lubricant and contribute to the rearrangement and orientation of the GFs under the sintering pressure, so that the angle between the orientation of the GCus and the X–Y direction gradually decreased with the increase of Cu content on the surface of the
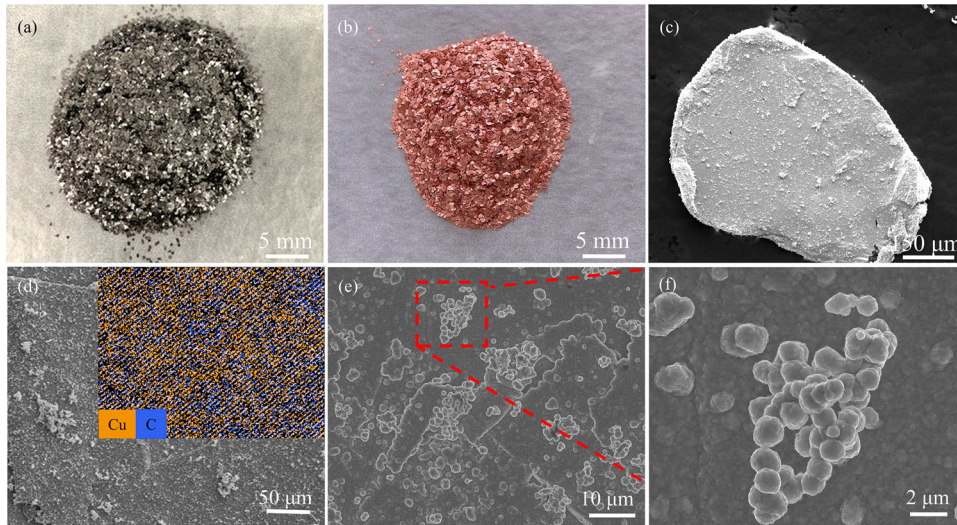
Fig. 2. Morphologies of a GF before and after electroless plating: (a) before plating; (b) after plating; (c) microscopic morphology of Cu-coated GF; (d) EDS mapping result; (e, f) morphology and magnification views of the Cu coating on the GF.
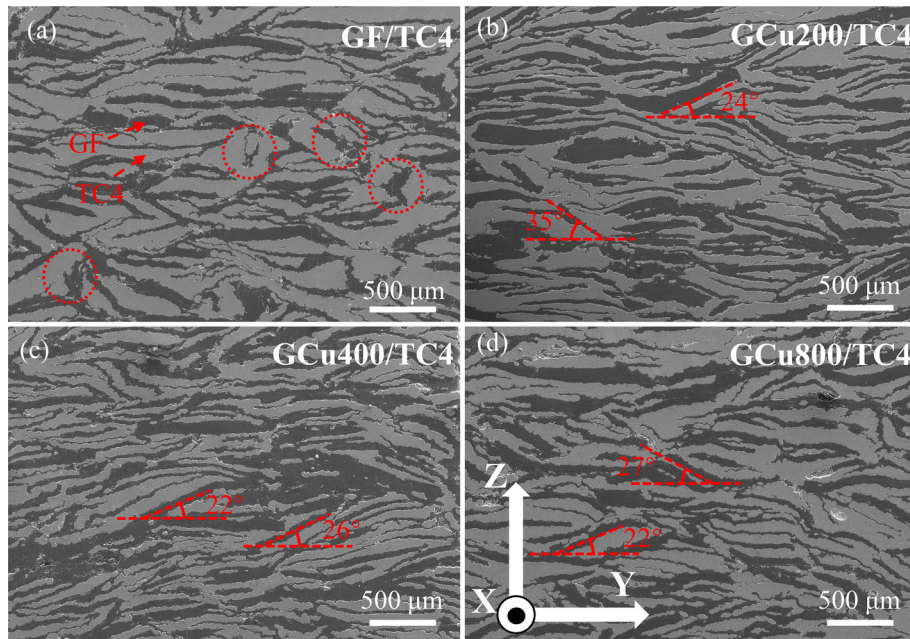

Fig. 3. SEM images of GCu/TC4 composites with different plating thicknesses sintered at 1150°C: (a) GF/TC4; (b) GCu200/TC4; (c) GCu400/TC4; and (d) GCu800/TC4.

GFs. However, when the thickness of Cu coating reached a certain amount, its lubrication effect became not significant enough, so the angle change between the GCus orientation and X–Y direction was not obvious.

The effect of sintering temperature on the orientation of the GCus in the corresponding composite (GCu400/TC4) was studied when the thickness of the Cu coating was fixed at 1.3 μm. Figure 4 shows the SEM images of GCu400/TC4 obtained at different sintering temperatures. It can be seen that the distribution of the GCus in the TC4 matrix was relatively uniform, and there was no direct stacking

contact between the GCus. However, by further observing the orientation of the GCus, it can be seen that there was an angle between the orientation direction of some GCus and the X–Y direction in all the samples. In particular, it was observed that the maximum angle between the GCu orientation and the X–Y direction reached an average of 46° in the composite sintered at 1050°C (Fig. 4a). With the increase of sintering temperature, as shown in Fig. 4b–d, it can be seen that the angle decreased gradually. When the sintering temperature increased to 1200°C, the angle changed slightly. The change of angle with temperature was related

Thermal Conductivity and Microstructure of Cu-Coated Graphite Flake/Ti Alloy Composites Fabricated by Spark Plasma Sintering
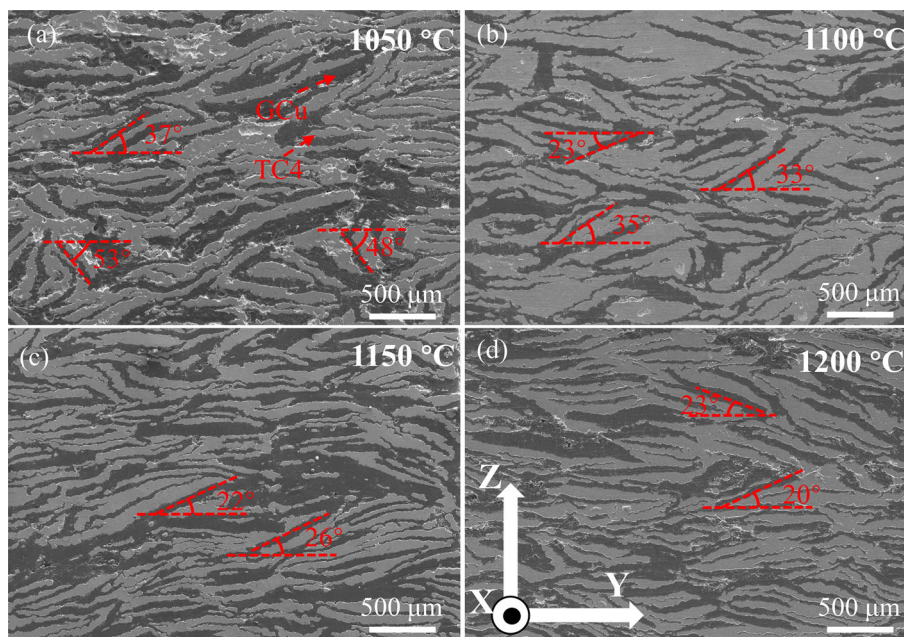
1267

Fig. 4. SEM images of GCu400/TC4 composites sintered at different temperatures: (a) 1050°C; (b) 1100°C; (c) 1150°C; and (d) 1200°C.

to the fluidity of the Cu after melting at different temperatures and the deformation resistance of the TC4 matrix at different temperatures. After the Cu melted into the liquid phase, its fluidity increased with the increase of sintering temperature, while the deformation resistance of the TC4 matrix decreased with the increase of temperature, which reduced the resistance of the GCus to a parallel arrangement under pressure. Therefore, with the increase of sintering temperature, the GCus were easier to arrange in the direction parallel to the X–Y direction under the action of sintering pressure in the Z direction.

The continuity of the GFs as calculated is shown in supplementary Table S-III. It is worth noting that the continuity ranged from 0.270 to 0.373, and that low continuity values represent less M–M contacts. Moreover, the continuity varied significantly with sintering temperature and the thickness of the coating. This is understandable because, as the sintering temperature and coating thickness increased, the bending phenomenon of the GFs and the angle between the GFs and the X–Y direction decreased, gradually tending to a parallel arrangement. This meant that the probability of mutual contact between the GFs decreased, and their dispersion in the matrix was better, which meant that the continuity of the flake graphite was reduced. The results of the continuity calculations show that the previous analysis of the influence of sintering temperature and coating thickness variations on the orientation of the GFs is reasonable.

The XRD results of the GF/TC4, GCu200/TC4, GCu400/TC4, and GCu800/TC4 composites sintered at 1150°C are shown in Fig. 5. The results indicate that the diffraction peaks of the matrix phase, the
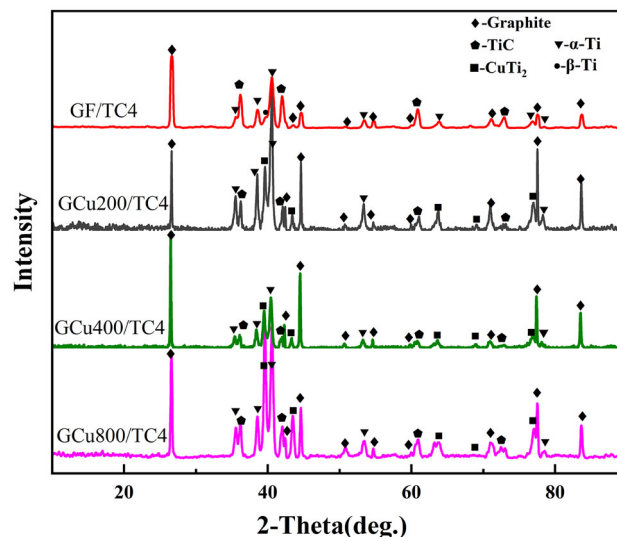

Fig. 5. XRD patterns of GF/TC4 and GCu/TC4 composites with different Cu plating thicknesses prepared at 1150°C.

reinforcement phase, and the diffraction peaks of TiC were detected in all the composites. In addition, by comparing the diffraction patterns of the GF/TC4 and GCu/TC4 composites in Fig. 5, it can be seen that all the GCu/TC4 composites corresponding to different Cu coating thicknesses showed diffraction peaks of $CuTi_2$, which indicated that the TC4 matrix reacted with the GFs and the Cu, respectively.

In order to study the effect of the Cu plating layer on the interface between the GFs and the matrix in the composites, the interface between GF(GCu) and TC4 in the GF/TC4 and GCu400/TC4 composites was observed and characterized by TEM. The TEM images of the GF/TC4 composites are shown in

Fig. 6. Figure 6c shows the selected area electron diffraction (SAED) pattern corresponding to the A region in Fig. 6a, which was determined to be a GF by diffraction spots calibration. The diffraction spots of area B in Fig. 6a are shown in Fig. 6d, from which it can be determined that this layer was a TiC layer. In addition, fine gaps between the GFs and the TiC layers can be observed in Fig. 6a. In Fig. 6b, it can be seen that the TiC layer was not dense, and that there were pores in it. The existence of such pores and gaps is not conducive to heat transfer of the interface, and will inevitably affect the TC of the composite.

The TEM image of the GCu400/TC4 composite and the EDS mapping results of the elements are shown in Fig. 7. The two red dashed lines in Fig. 7 mark the interfaces between GCu and TiC and between TiC and TC4, respectively. It can be seen that the combination of the two interfaces was good, and that no obvious gaps were observed along the interfaces. By comparing the morphology of the TiC layer in the GF/TC4 composite fabricated at the same sintering temperature, as shown in Fig. 6, it can be seen that the pores in the TiC layer in the GCu/TC4 composite were significantly reduced.

The EDS mapping results of elements at the interface and the composition results of four points B, C, D, and E in Fig.7a listed in Table I indicate that the Cu element has diffused into the TC4 matrix. and $CuTi_2$ phase can be observed at the interface between TiC and the TC4 matrix, which is consistent with the XRD results. Due to the low melting point of Cu (1083°C),[39] Cu was easy to diffuse into the matrix at the temperature set in the experiment, which promoted the sintering densification, significantly reduced the pores in the TiC layer, and improved the interface bonding between the GFs and the TC4 matrix.

The thickness of the TiC layers and morphologies of the interfaces in the GF/TC4 composite and the GCu/TC4 composites with different plating thicknesses fabricated at 1150°C are shown in Fig. 8. Figure 8b–d shows the morphology of the interfaces in the composites. The darker (black) area was GF (GCu), the brighter (light gray) area was TC4, and the dark gray layer was the interface reaction product TiC layer. The matrix TC4 regions of the samples were composed of the α and β phases. For the composites prepared under each experimental condition, fields of view with the same magnification were selected in three different areas, and then ten different positions in each field of view were randomly chosen to measure the thickness of the TiC layer. Finally, the average value was taken as the thickness of the TiC layer under the experimental conditions, as shown in Fig. 8a. The thickness of the TiC layer in the GF/TC4 composite was 4.8 μm. The thicknesses of the TiC layers in the GCu200/TC4, GCu400/TC4, and GCu800/TC4 composites were 1.2, 1.1, and 0.9 μm, respectively. By comparing the changes in the thickness of the TiC layers, it can be concluded that the thickness of the TiC layer the in the composite material was significantly reduced after coating Cu on the surface of the GFs, and the that the thicker the Cu coating, the smaller the thickness of the TiC layer.

Because the formation free energy of a carbon/Ti system is low (-184 kJ mol^{-1} at 298 K),[40] the TiC phase is easily formed at the interface between the reinforcement phase and the Ti. The diffusion rate of C atoms through the TiC layer into the matrix was approximately four orders of magnitude higher than that of Ti atoms through TiC,[41] so it can be inferred that the growth of the TiC layer between the GFs and the TC4 matrix was mainly controlled by the diffusion of C atoms in the GFs through the formed TiC. Since the wettability of Cu and C was poor and no reaction occurred, when there was Cu between the GFs and the TC4 interface, except for a small amount of Cu that would fill the lamellar gap inside the GFs, the diffusion of Cu into the TC4 matrix was dominant in the sintering process. When all the Cu diffused into the matrix, the GFs and the TC4 matrix began to contact each other directly, so the presence of the Cu coating can delay the time of direct contact between the GFs and the matrix. In a given sintering time, the longer the delayed contact time, the shorter the direct contact time, which meant that a thinner TiC layer formed by the reaction between the matrix and the GFs.
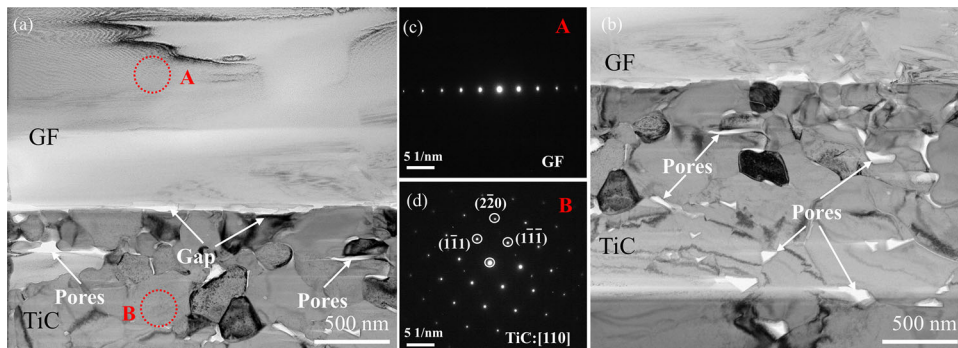

Fig. 6. (a) and (b) TEM images of GF/TC4 composites prepared at 1150°C; (c) and (d) selected area electron diffraction (SAED) patterns of the circular area marked with points *A* and *B* in (a).
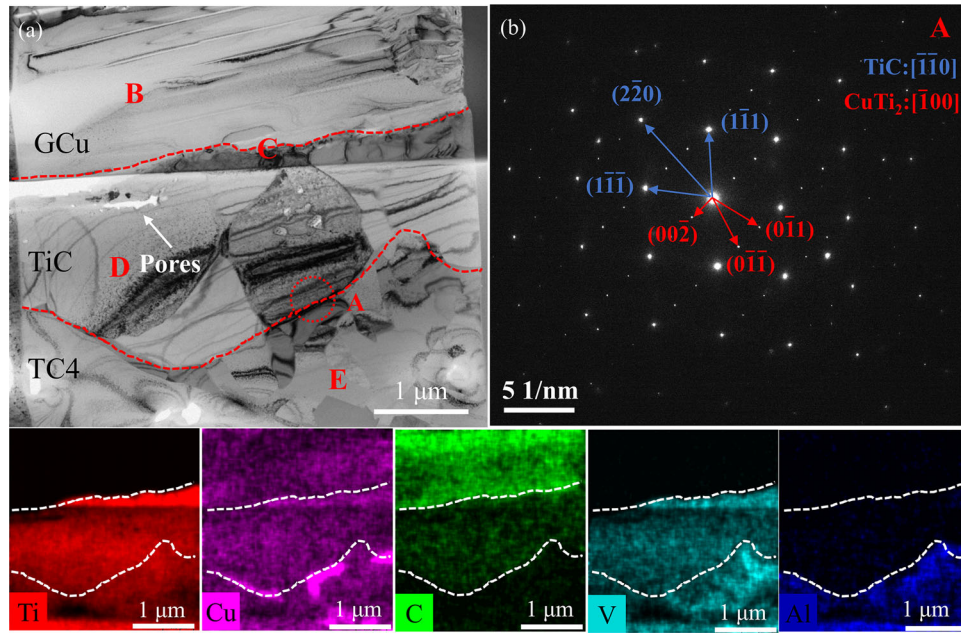
Fig. 7. (a) TEM images and EDS mappings at the interface of GCu400/TC4 composites prepared at 1150°C; (b) SAED pattern of the corresponding region in (a).

Table I. EDS results for four points marked B–E in Fig. 7

Point position	C (at.%)	Ti (at.%)	Al (at.%)	V (at.%)	Cu (at.%)
B	92.19	0.08	0.00	0.01	7.72
C	28.08	58.87	0.06	0.43	12.56
D	46.72	41.72	0.13	0.20	11.23
E	5.82	49.76	4.99	11.67	36.07

The thicker the Cu coating on GF surface, the longer it took for it to fully diffuse into the TC4 matrix; that is, the time for direct contact between the matrix and the GFs decreased with the increase of the Cu coating thickness. Therefore, as shown in Fig. 8a, it is reasonable that the thickness of the TiC layer decreased with the increase of the Cu coating thickness.

To investigate the effect of different sintering temperatures on the thickness of the TiC layer at the interface in the GCu/TC4 composites, the thickness of layer in the GCu400/TC4 composites sintered at different temperature was measured, as shown in Fig. 9a, in which the thickness of the layer sintered at 1050°C was 0.9 μm. With the sintering temperature increased to 1150°C, the thickness of the TiC layer increased to 1.1 μm. When the temperature was further increased to 1200°C, the thickness of the TiC layer increased sharply to 1.6 μm. With the increase of sintering temperature, the thickness of TiC increased gradually. This is mainly caused by, first, the growth of the TiC layer between the GCu and the TC4 matrix was affected by the time that the Cu coating delayed the interface reaction between the GFs and the TC4 matrix. At different sintering temperatures, Cu coatings with the same thickness had different delay times for interface reactions. The higher the temperature, the shorter the time for Cu to diffuse into the TC4 matrix; that is, the longer the time for interface reaction. In this way, the thickness of TiC increased with the increase of temperature. Second, the thickness of the TiC layer was controlled by the diffusion rate of C atoms in the TiC layer. The higher the temperature, the higher the diffusion rate. This also intensified the interface reaction, resulting in an increase in the thickness of the TiC layer. Under the combined action of these two reasons, the thickness of the TiC layer increased with the increase of temperature under the same Cu coating thickness.

Based on the results of Figs. 6, 7, 8, and 9, a schematic of the diffusion mechanism that modulated the thickness of the TiC layer at the interface of the GFs and the TC4 is shown in Fig. 10. As shown in Fig. 10a, if a GF was directly mixed with TC4 during the sintering process, C atoms would diffuse into the TC4 matrix to form a TiC layer. As the sintering
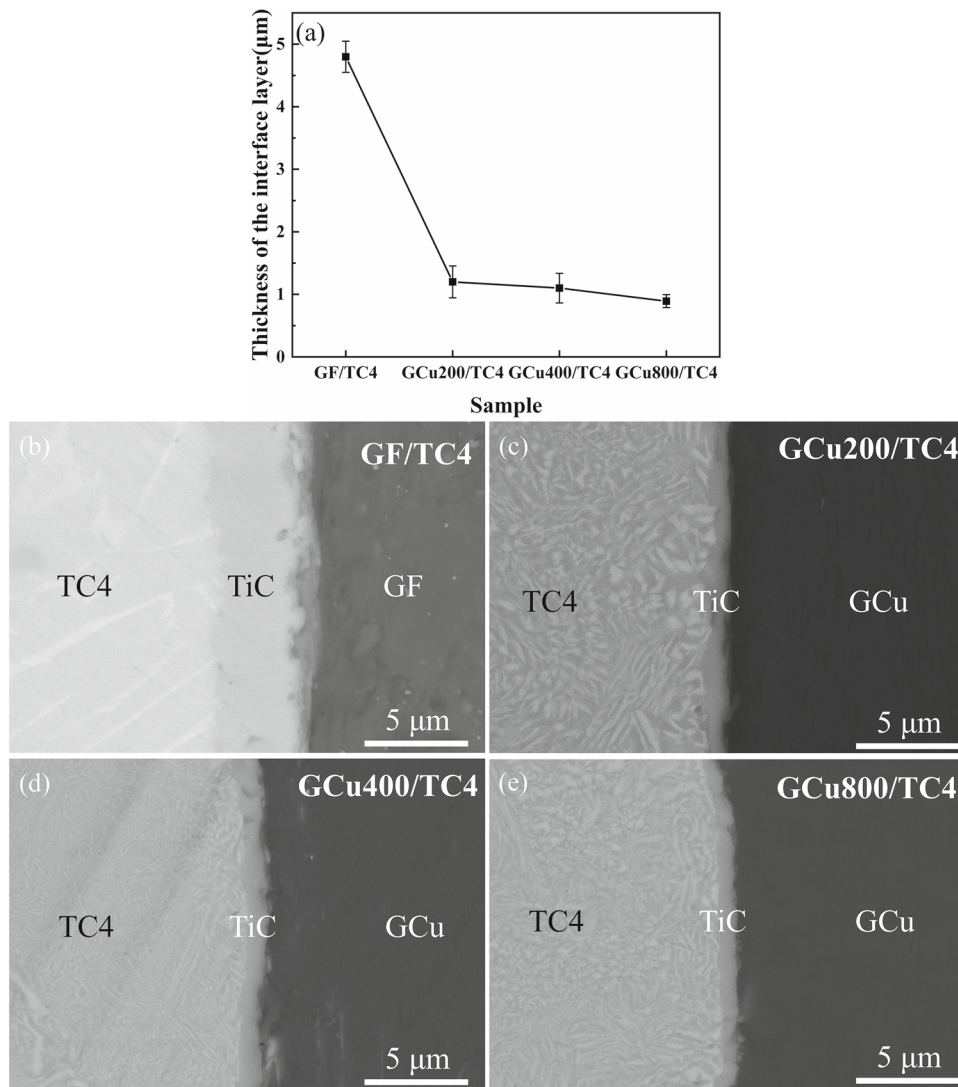
Fig. 8. (a) Thickness of TiC layers in GF/TC4 and GCu/TC4 composites with different plating thicknesses fabricated at 1150°C; SEM images of the interface in composites fabricated at 1150°C: (b) GF/TC4, (c) GCu200/TC4, (d) GCu400/TC4, and (e) GCu800/TC4.

proceeded, C atoms would continuously pass through the formed TiC layer and diffuse into the titanium matrix, resulting in a continuous increase in the thickness of the TiC layer with the prolongation of sintering time. Therefore, under the given sintering time conditions, after the composite material was sintered and densified, there would be a certain thickness of the TiC layer in the GF/TC4 composite. If a certain thickness of Cu was pre-coated on the surface of the GF (Fig. 10b), Cu would first diffuse gradually into the TC4. After the Cu was consumed, mutual contact between the GF and the TC4 substrate would occur. The presence of the Cu coating delayed the direct contact time between the GF and the matrix, which could significantly reduce the thickness of the TiC layer. In addition, the diffusion of Cu could promote sintering densification and reduce the pores and gaps at the interface.

Thermal Conductivities (TCs) of Composites

Figure 11a shows the TCs in the X–Y and Z directions of the composites corresponding to GFs with different Cu coating thicknesses fabricated at 1150°C. It can be seen that, with the increase of the Cu coating thickness from 0 to 1.3 μm, the TC of the corresponding composite increased sharply from 185.03 W m^{-1} K^{-1} to 230.12 W m^{-1} K^{-1}. With the further increase of the Cu coating thickness to 2.1 μm, the increase of the TC was not significant. The variation of TC in the Z direction with Cu coating thickness showed a similar law to that in the X–Y direction. In addition, the TC of the composite in the Z direction was much smaller than that in the X–Y direction. This anisotropy was determined by the characteristics of the GF itself, that is, the TC of the GF in the Z direction was far less than that in the X–Y direction.

Thermal Conductivity and Microstructure of Cu-Coated Graphite Flake/Ti Alloy Composites Fabricated by Spark Plasma Sintering
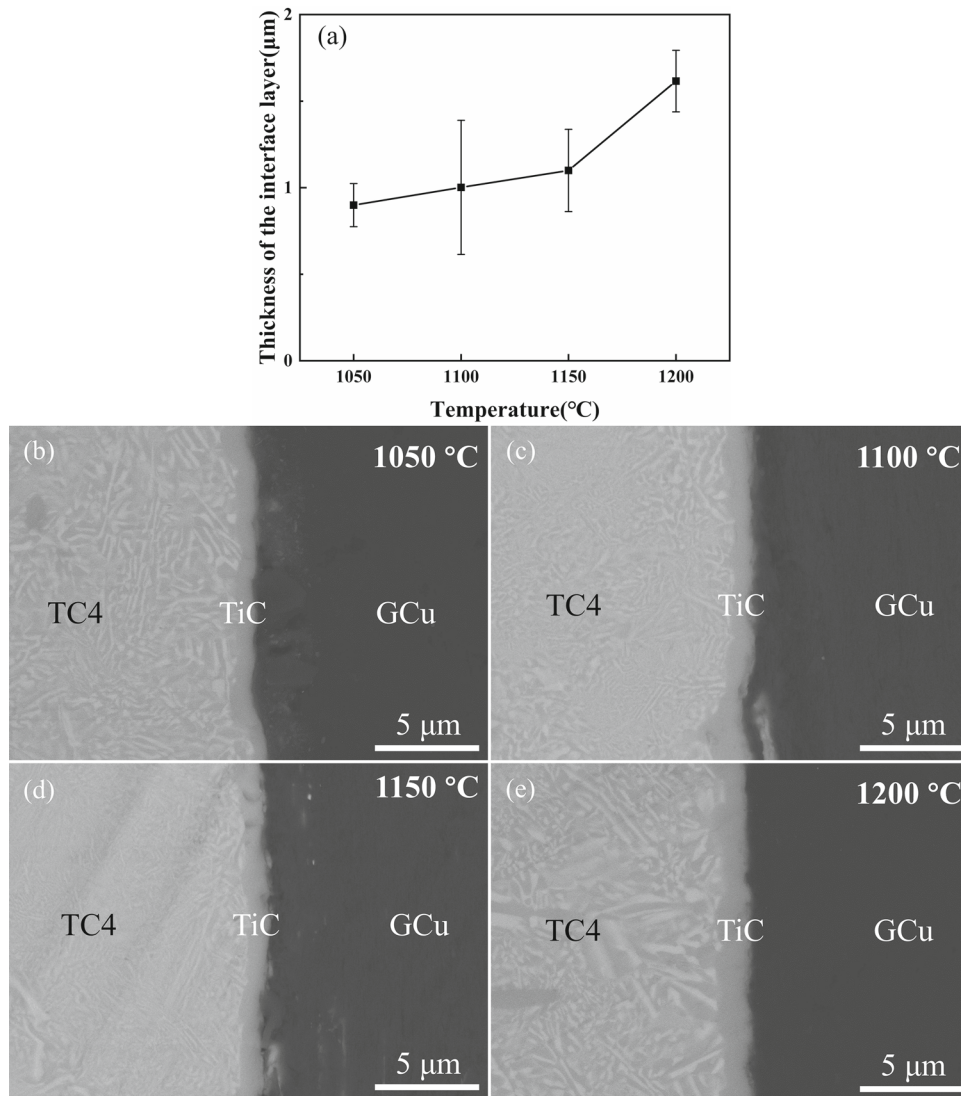
1271

Fig. 9. (a) Thickness of TiC layers in GCu400/TC4 composites sintered at different temperatures: SEM images of the interface in GCu400/TC4 composites sintered at different temperatures: (b) 1050°C, (c) 1100°C, (d) 1150°C, and (e) 1200°C.

Figure 11b shows the TCs in the X–Y and Z directions of GCu400/TC4 composites fabricated at different temperatures. In the range of 1050–1150°C, the TC of the composites in the X–Y direction increased with the increase of the sintering temperature. When the sintering temperature was 1150°C, the TC of the composite in the X–Y direction was the largest, which was 230.12 W m^{-1} K^{-1}. When the sintering temperature was increased to 1200°C, the TC in the X–Y direction decreased. The TC of the GCu400/TC4 composites in the Z direction decreased with the increase of sintering temperature.

The influence of coating thickness and temperature on the TC may be the result of the combined effect of the orientation of the GFs, the sintering density, and the thickness of the interface layer. First, as a high-TC material, the GFs exhibited excellent TC in the X–Y plane, but low TC in the Z direction (X–Y: 1000 W m^{-1} K^{-1}, Z: 30 W m^{-1} K^{-1}).[15,32,39,42] The anisotropic reinforcement with a low TC in one direction can affect the effective TC of the composites to a larger extent.[43,44] Therefore, the orientation of GFs close to the parallel alignment with the X–Y direction was favorable to improve the TC of the composite in the X–Y direction. Secondly, for metal matrix composites with high TC, the heat transfer is mainly conducted by free electrons and lattice vibrations. If there are pores and other defects at the interface between the GFs and TC4 or in the composite during heat transfer, phonon and electron scattering occurs within the defects, resulting in the reduction of the TC.[21,32] Therefore, increasing the density of the composite or improving the interface bonding can increase the TC of the composite. Finally, the interfacial thermal resistance was proportional to the thickness of the carbide layer.[21,45] Therefore,
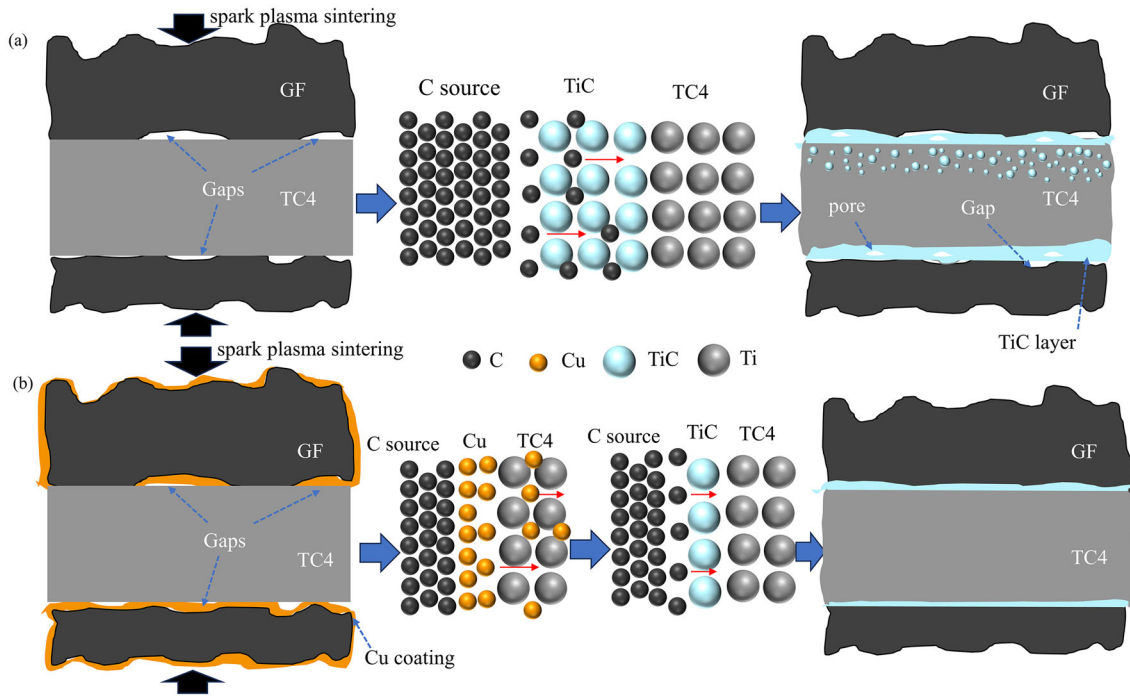
Fig. 10. Schematic of the diffusion mechanism that regulates the thickness of the TiC layer at the interface of the composite: (a) GF/TC4, and (b) GCu/TC4.
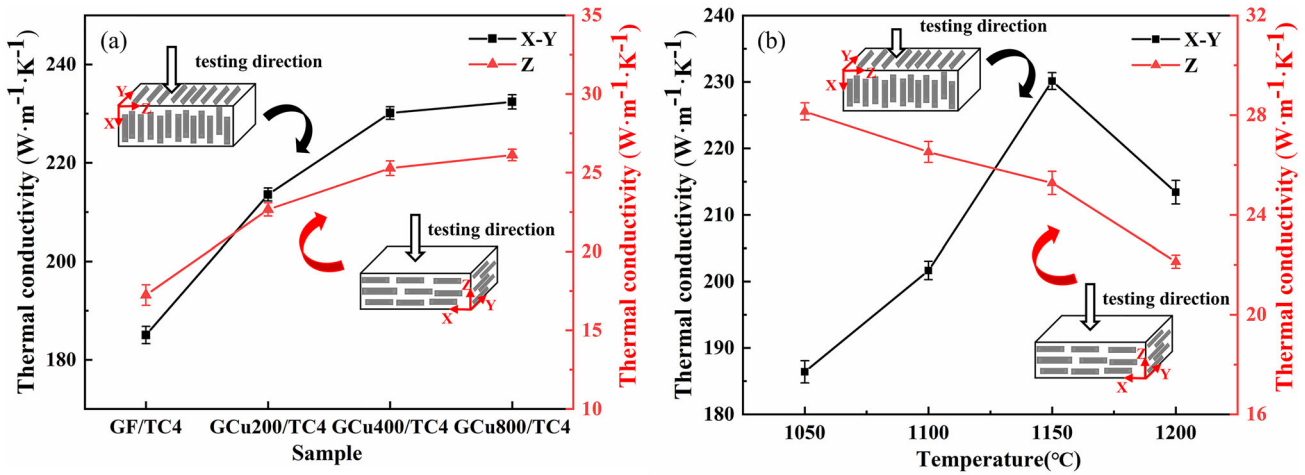

Fig. 11. (a) TCs of the GF/TC4 composite and GCu/TC4 composites with different plating thicknesses fabricated at 1150°C; (b) TCs of GCu400/TC4 composites fabricated at different temperatures.

the thicker the TiC layer, the higher the interface thermal resistance, resulting in a lower TC of the composite.

It can be seen from the previous results that the Cu coating on the GF surface had a significant effect on the thickness of the interface product, TiC, the density of interface layer, and the orientation of the GFs. As mentioned above, the Cu on the surface of the GFs mainly underwent two processes during sintering. First, it transformed into a liquid phase at high temperature. In this process, it acted as a lubricant and promoted the rearrangement of the

GFs. The higher the temperature, the better the fluidity of the Cu, which made the orientation of the GFs more and more consistent, thus conducive to improving the TC of the composite in the X–Y plane direction. In the Z direction, as the orthogonal decomposition amount of TC in the X–Y direction decreased, the TC in the Z direction became smaller as the GF orientation gradually approached consistency with the X–Y direction. In addition, the molten Cu can be used as a sintering aid to improve the diffusion of the matrix Ti and further improve the density of the composite and interface layer (see

Thermal Conductivity and Microstructure of Cu-Coated Graphite Flake/Ti Alloy Composites Fabricated by Spark Plasma Sintering

1273

supplementary Table S-IV), thus increasing the TC of composite. After Cu melting, it would gradually diffuse into the TC4 matrix as the sintering proceeded, which is the second stage. The higher the temperature, the faster the diffusion rate of the Cu. When the total amount of Cu was fixed, the faster the consumption rate, the shorter time it delayed the contact between the matrix and the GFs. That is, the contact time between the GFs and the TC4 matrix lengthened with the increase of temperature in the same sintering time. Therefore, the thickness of the TiC layer at the interface increased with the increase of sintering temperature. In addition, the rapid diffusion of C atoms at high temperature also caused the thickness of the TiC layer at the interface to further increase with the increase of sintering temperature. In the second stage, when the sintering temperature was fixed, with the increase of Cu plating thickness on the surface of the GFs, the time for its complete diffusion into the TC4 matrix became longer, so the time for delaying the contact between the matrix and GF became longer. As a result, the thickness of TiC at the interface decreased gradually with the increase of Cu plating thickness. The decrease of TiC thickness reduced the interfacial thermal resistance and thus increased the TC of the composite. In other words, after coating Cu on the surface of the GFs, it was beneficial to its consistent orientation in the TC4 matrix, further improving the sintering density, and reducing the thickness of the interface layer. Therefore, this shows that the TC of the composite in the X–Y and Z directions in Fig. 11a increased with the increase of the Cu coating thickness.

As for the influence of sintering temperature on the TC in Fig. 11b, based on the analysis of the thickness of interface layer TiC, theoretically, the TC should decrease with the increase of sintering temperature. However, as previously analyzed, the TC of the composites was affected by the thickness of the interface layer, the orientation of the GFs, and the density of the composite. Below 1150°C, the TC in the X–Y direction of the composites increased with the increase of sintering temperature. This meant that the positive effect on TC caused by the more consistent orientation of the GCu and increased density was greater than the negative effect on TC caused by the increased thickness of the interface layer; When the temperature was 1200°C, the negative effect of thickness of the interface layer on the TC was dominant, so the TC became smaller at this temperature. For the TC of the composite in the Z direction, it gradually decreased due to the more consistent orientation of the GCu and the increasing thickness of the TiC layer.

Under the experimental conditions of this study, the pre-plating of Cu on the surface of the GFs improved the interface bonding between the GFs and the TC4, significantly reduced the thickness of the TiC, and finally increased the TC of the 50 vol.% GF/TC4 composite by 25%, reaching 232.4 W m^{-1} K^{-1} in the X–Y direction. The high TC makes the GF/TC4 composites suitable candidates for heat transfer materials used in offshore engineering. Next, we will focus on the mechanical properties and corrosion resistance of the composite.

CONCLUSION

1. GF/Ti and GCu/TC4 composites were fabricated by SPS. The interface reaction occurred in both kinds of composites, and TiC layers were formed. The thickness of the TiC layer gradually increased with the increase of sintering temperature. The introduction of Cu plating slowed the interface reaction, the thickness of the TiC layer was reduced by 80%, the pores inside the TiC layer were reduced, and the interface bonding was improved.

2. After coating Cu on the surface of the GFs, the interfacial thermal resistance was significantly reduced. The TC of the composite in the X–Y direction was increased from 185.03 W m^{-1} K^{-1} to 232.4 W m^{-1} K^{-1}, while the TC of the composite in the Z direction was increased from 17.2 W m^{-1} K^{-1} to 26.1 W m^{-1} K^{-1}.

3. The TC of the GCu400/TC4 composites in the X–Y direction gradually increased with the increase of sintering temperature from 1050 to 1150°C and then decreased after further increase of the temperature to 1200°C. The TC of the GCu400/TC4 composites in the Z direction gradually decreased with the increase of sintering temperature. This was due to the different effects of the density, the orientation of the GFs, and the interface reaction layer thickness on the TC of the composites at different sintering stages.

SUPPLEMENTARY INFORMATION

The online version contains supplementary material available at https://doi.org/10.1007/s11837-023-06288-2.

AUTHOR CONTRIBUTIONS

ZY: Investigation, Formal analysis, Data curation, Writing—original draft. JQ: Formal analysis, Writing—review & editing. WZ: Formal analysis, Writing—review & editing. XR: Formal analysis, Writing—review & editing. YZ: Formal analysis, Writing—review & editing. SR: Conceptualization, Supervision, Writing—review & editing, Resources, Project administration. XQ: Resources, Supervision.

FUNDING

CONFLICT OF INTEREST

On behalf of all authors, the corresponding author states that there is no conflict of interest.

REFERENCES

1. M.M. Abu-Khader, *Renew. Sust. Energ. Rev.* 12, 2012 https://doi.org/10.1016/j.rser.2012.01.009 (1883).
2. J. Zhang, X. Zhu, M.E. Mondejar, and F. Haglind, *Renew. Sust. Energ. Rev.* 101, 305 https://doi.org/10.1016/j.rser.2018.11.017 (2019).
3. A.S. Pelliccione, R. Santanna, M.H.S. Siqueira, A.F. Ribeiro, J.E. Ramos, O.P. Silva, and M.F. Pimentel, *Eng. Fail. Anal.* 105, 1172 https://doi.org/10.1016/j.engfailanal.2019.07.059 (2019).
4. N.S. Pandya, H. Shah, M. Molana, and A.K. Tiwari, *Eur. J. Mech. B Fluids* 81, 173 https://doi.org/10.1016/j.euromechflu.2020.02.004 (2020).
5. A. Abbas, H. Lee, A. Sengupta, and C. Wang, *Appl. Therm. Eng.* 167, 114705 https://doi.org/10.1016/j.applthermaleng.2019.114705 (2020).
6. S.A. Zahrani, M.S. Islam, and S.C. Saha, *Energy Procedia* 160, 597 https://doi.org/10.1016/j.egypro.2019.02.211 (2019).
7. B. Jin, J. Lee, M. Park, T. Yun, Y. Song, and I. Kim, *Procedia Eng.* 174, 171 https://doi.org/10.1016/j.proeng.2017.01.197 (2017).
8. X.N. Mu, H.N. Cai, H.M. Zhang, Q.B. Fan, F.C. Wang, Z.H. Zhang, Y. Wu, Y.X. Ge, S. Chang, R. Shi, Y. Zhou, and D.D. Wang, *Mater. Sci. Eng. A.* 725, 541 https://doi.org/10.1016/j.msea.2018.04.056 (2018).
9. X.N. Mu, H.M. Zhang, P.W. Chen, X.W. Cheng, L. Liu, Y.X. Ge, N. Xiong, and Y.C. Zheng, *Carbon* 175, 334 https://doi.org/10.1016/j.carbon.2021.01.113 (2021).
10. Y. Guo, K. Yu, J. Niu, M. Sun, G. Dai, Z. Sun, and H. Chang, *J. Mater. Res. Technol.* 15, 6871 https://doi.org/10.1016/j.jmrt.2021.11.109 (2021).
11. S. Mahmood, R.U. Din, M. Khan, M. Shahzad, M.F. Khan, S. Akhtar, A. Mateen, and A. Wadood, *Mater. Chem. Phys.* https://doi.org/10.1016/j.matchemphys.2022.126142 (2022).
12. Y.C. Zhang, T. Mabrouki, D. Nelias, and Y.D. Gong, *Finite Elem. Anal. Des.* 47, 850 https://doi.org/10.1016/j.finel.2011.02.016 (2011).
13. A. Saini, B.S. Pabla, and S.S. Dhami, *Proc. Inst. Mech. Eng. Part B* 230, 2016 https://doi.org/10.1177/0954405416640176 (1977).
14. X.Y. Gu, C.Y. Dong, and T. Cheng, *Appl. Math. Model.* 56, 517 https://doi.org/10.1016/j.apm.2017.12.028 (2018).
15. C. Xue, H. Bai, P.F. Tao, J.W. Wang, N. Jiang, and S.L. Wang, *Mater. Des.* 108, 250 https://doi.org/10.1016/j.matdes.2016.06.122 (2016).
16. Y. Sohn, T. Han, and J.H. Han, *Carbon* 149, 152 https://doi.org/10.1016/j.carbon.2019.04.055 (2019).
17. Z. Shen, G. Ji, A. Addad, C. Labrugere, Y. Lu, and J. Silvain, *Diamond Relat. Mater.* 118, 108513 https://doi.org/10.1016/j.diamond.2021.108513 (2021).
18. C. Zhou, W. Huang, Z. Chen, G. Ji, M.L. Wang, D. Chen, and H.W. Wang, Compos. *B. Eng.* 70, 256 https://doi.org/10.1016/j.compositesb.2014.11.018 (2015).
19. X.Y. Liu, W.G. Wang, D. Wang, D.R. Ni, L.Q. Chen, and Z.Y. Ma, *Mater. Chem. Phys.* 182, 256 https://doi.org/10.1016/j.matchemphys.2016.07.030 (2016).
20. J. Chen, S. Ren, X. He, and X. Qu, *Carbon* 121, 25 https://doi.org/10.1016/j.carbon.2017.05.082 (2017).
21. L. Wang, J. Li, M. Catalano, G. Bai, N. Li, J. Dai, X. Wang, H. Zhang, J. Wang, and M.J. Kim, *Compos. Part A Appl. Sci.*
22. P. Jamzad, J. Kenna, and M. Bahrami, *Int. J. Heat Mass Transf.* 131, 1205 https://doi.org/10.1016/j.ijheatmasstransfer.2018.11.129 (2019).
23. Y. Zhang, H.L. Zhang, J.H. Wu, and X.T. Wang, *Scr. Mater.* 65, 1097 https://doi.org/10.1016/j.scriptamat.2011.09.028 (2011).
24. X. Shen, X. He, S. Ren, H. Zhang, and X. Qu, *J. Alloys Compd.* 529, 134 https://doi.org/10.1016/j.jallcom.2012.03.045 (2012).
25. C. Zhang, Z. Cai, Y. Tang, R. Wang, C. Peng, and Y. Feng, *Diamond Relat. Mater.* 86, 98 https://doi.org/10.1016/j.diamond.2018.04.020 (2018).
26. X. Liu, J. Mao, P. Liu, and X. Wei, *Carbon* 49, 477 https://doi.org/10.1016/j.carbon.2010.09.044 (2011).
27. M. Li and X. Lei, *Comput Mater. Sci.* 211, 111487 https://doi.org/10.1016/j.commatsci.2022.111487 (2022).
28. E. Neubauer, M. Kitzmantel, M. Hulman, and P. Angerer, *Compos. Sci. Technol.* 70, 2228 https://doi.org/10.1016/j.compscitech.2010.09.003 (2010).
29. K. Chu, Q. Wu, C. Jia, X. Liang, J. Nie, W. Tian, G. Gai, and H. Guo, *Compos Sci. Technol.* 70, 298 https://doi.org/10.1016/j.compscitech.2009.10.021 (2010).
30. L. Jiang, Z. Li, G. Fan, L. Cao, and D. Zhang, *Carbon* 50, 2012 https://doi.org/10.1016/j.carbon.2011.12.057 (1993).
31. N. Chamroune, D. Mereib, F. Delange, N. Caillault, Y. Lu, J. Grosseau-Poussard, and J. Silvain, *J. Mater. Sci.* 53, 8180 https://doi.org/10.1007/s10853-018-2139-1 (2018).
32. Y. Zhao, S. Ren, Q. Liu, J. Chen, X. He, and X. Qu, *J. Alloys Compd.* 815, 152425 https://doi.org/10.1016/j.jallcom.2019.152425 (2020).
33. R. Prieto, J.M. Molina, J. Narciso, and E. Louis, *Scr. Mater.* 59, 11 https://doi.org/10.1016/j.scriptamat.2008.02.026 (2008).
34. H. Bai, C. Xue, J.L. Lyu, J. Li, G.X. Chen, J.H. Yu, C.T. Lin, D.J. Lv, and L.M. Xiong, *Compos. Part A Appl. Sci. Manuf.* 106, 42 https://doi.org/10.1016/j.compositesa.2017.11.019 (2018).
35. T. Wejrzanowski, M. Grybczuk, M. Wasiluk, and K.J. Kurzydlowski, *AIP Adv.* 5, 077142 https://doi.org/10.1063/1.4927389 (2015).
36. J.N. Ma, L. Bolzoni, and F. Yang, *J. Alloys Compd.* 868, 17 https://doi.org/10.1016/j.jallcom.2021.159182 (2021).
37. T. Wejrzanowski, M. Grybczuk, M. Chmielewski, K. Pietrzak, K.J. Kurzydlowski, and A. Strojny-Nedza, *Mater. Des.* 99, 163 https://doi.org/10.1016/j.matdes.2016.03.069 (2016).
38. J. Michalski, T. Wejrzanowski, S. Gierlotka, J. Bielinski, K. Konopka, T. Kosmac, and K.J. Kurzydlowski, *J. Eur. Ceram. Soc.* 27, 831 https://doi.org/10.1016/j.jeurceramsoc.2006.04.034 (2007).
39. T. Ueno, T. Yoshioka, J. Ogawa, N. Ozoe, K. Sato, and K. Yoshino, *Synth. Met.* 159, 2170 https://doi.org/10.1016/j.synthmet.2009.10.006 (2009).
40. X.N. Mu, H.M. Zhang, H.N. Cai, Q.B. Fan, Z.H. Zhang, Y. Wu, Z.J. Fu, and D.H. Yu, *Mater. Sci. Eng. A.* 687, 164 https://doi.org/10.1016/j.msea.2017.01.072 (2017).
41. Y. Choi and S.W. Rhee, *J. Mater. Sci.* 30, 4637 https://doi.org/10.1007/BF01153073 (1995).
42. C. Zhou, G. Ji, Z. Chen, M. Wang, A. Addad, D. Schryvers, and H. Wang, *Mater. Des.* 63, 719 https://doi.org/10.1016/j.matdes.2014.07.009 (2014).
43. J.C. Lloyd, E. Neubauer, J. Barcena, and W.J. Clegg, *Compos. Sci. Technol.* 70, 2284 https://doi.org/10.1016/j.compscitech.2010.05.002 (2010).
44. Q. Liu, X. He, S. Ren, T. Liu, Q. Kang, and X. Qu, *J. Mater. Sci.* 48, 5810 https://doi.org/10.1007/s10853-013-7373-y (2013).
45. L. Yang, L. Sun, W. Bai, and L. Li, *Diamond Relat. Mater.* 94, 37 https://doi.org/10.1016/j.diamond.2019.02.014 (2019).
46. D. Janas, A. Cabrero-Vilatela, J. Bulmer, L. Kurzepa, and K.K. Koziol, *Carbon* 64, 305 https://doi.org/10.1016/j.carbon.2013.07.067 (2013).

Manuf. 113, 76 https://doi.org/10.1016/j.compositesa.2018.07.023 (2018).